Tetraammineruthenium(II) and -ruthenium(III) Complexes of *o*-Benzoquinone Diimine and Their Redox Series

Robert A. Metcalfe and A. B. P. Lever*

Department of Chemistry, York University, North York (Toronto), Ontario, Canada M3J 1P3

Received February 27, 1997[⊗]

The complexes $[Ru(NH_3)_4(4,5\text{-}R_2\text{-}bqdi)]^{n+}$ where bqdi is *o*-benzoquinone diimine, R = H, Cl, or OMe, and n = 2 or 3 have been characterized by elemental analysis, optical spectroscopy, electrochemistry, spectroelectrochemistry, and electron paramagnetic and nuclear magnetic resonance spectroscopies. ZINDO/S calculations provide a very detailed picture of the degree of mixing existing between metal and ligand orbitals. Both π back-donation and ligand $\pi-$d mixing are important such that these compounds are considered to be extensively delocalized. In the Ru^{III} systems compared with the Ru^{II} systems, ligand $\pi-$d mixing is somewhat more important and π back-donation somewhat less important. Assignments of the electronic spectra are presented in detail in terms of the degree of mixing in the various orbitals. Surprisingly, on the basis of the ZINDO analysis, the lowest energy, strong, visible-region band in the electronic spectra of the Ru^{III} species is shown to be predominantly MLCT and not LMCT as might have been assumed.

Introduction

The nature of the chemical bond in transition metal complexes has been a subject of great interest to us over the years. In recent times we have explored ruthenium complexes of so-called noninnocent or redox-active ligands, especially the quinonoid ligands,[1−4] a topic of fairly widespread general interest.[5] Ammine complexes of ruthenium have been used extensively in the development of the current understanding of the mixing between metal and ligand orbitals existing in transition metal complexes.[6] These species are interesting because the low-spin d^6 ruthenium(II) and d^5 ruthenium(III) are thought to act as π-electron donors and π-electron acceptors, respectively, and therefore can interact with both the π^* and the π systems of a variety ligands.

Most of our previous studies have used 2,2′-bipyridine as a counterligand because of the ease of formation of such complexes and the possibility of using pyridine as a spectroscopic and electrochemical marker. However this has limited our studies to Ru^{II} species, due to the high potentials required to generate the corresponding $[Ru^{III}(bpy)_2L]^{3+}$ complexes. Such bipyridine Ru^{III} complexes appear to be very unstable; indeed a $[Ru^{III}(bpy)_2L]^{3+}$ complex with the benzoquinone diimine ligand has never been isolated, or seen spectroscopically.

On the other hand, ruthenium tetraammine complexes of these quinonoid ligands can be produced in the Ru^{II} or Ru^{III} oxidation state, due to the ability of the σ-donor NH_3 ligands to stabilize the Ru^{III} oxidation state. According to the electrochemical parameter theory,[7] the $Ru^{II}(NH_3)_4$ fragment is some 0.76 V easier to oxidize to Ru^{III} than is $Ru^{II}(bpy)_2$. The $Ru^{II}(NH_3)_4$ moiety should then be a much stronger σ- and π-base than $Ru^{II}(bpy)_2$. This class of compounds readily forms a redox series[1−5] where the quinone diimine (QH_2) can be reduced to a semiquinone diiminato(1−) (SqH_2) and to a diamido(2−) ($CatH_2$) or diamine(0) ($CatH_4$) species, the last two being related to the catecholate oxidation state of the normal quinone ligands. The H_2, H_4 designation indicates the number of N-bound H atoms. This nomenclature is used as a general abbreviation for the oxidation state of the ligand. While, in the bipyridine complexes, further reduction at the bipyridine ligands occurred,

* Corresponding author. E-mail: blever@yorku.ca.

⊗ Abstract published in *Advance ACS Abstracts,* September 15, 1997.

(1) Masui, H.; Lever, A. B. P.; Auburn, P. R. *Inorg. Chem.* **1991**, *30*, 2402. Masui, H.; Lever, A. B. P.; Dodsworth, E. S. *Inorg. Chem.* **1993**, *32*, 258.

(2) Lever, A. B. P.; Masui, H.; Metcalfe, R. A.; Stufkens, D. J.; Dodsworth, E. S.; Auburn, P. R. *Coord. Chem. Rev.* **1993**, *125*, 317.

(3) Metcalfe, R. A.; Dodsworth, E. S.; Lever, A. B. P.; Pietro, W. J.; Stufkens, D. J. *Inorg. Chem.* **1993**, *32*, 3581.

(4) Auburn, P. R.; Lever, A. B. P. *Inorg. Chem.* **1990**, *29*, 2551. da Cunha, C. J.; Fielder, S. S.; Stynes, D. V.; Masui, H.; Auburn, P. R.; Lever, A. B. P. *Inorg. Chim. Acta* **1996**, *241*, 293. Stufkens, D. J.; Snoeck, Th. L.; Lever, A. B. P. *Inorg. Chem.* **1988**, *27*, 953. Haga, M.; Dodsworth, E. S.; Lever, A. B. P.; Boone, S. R.; Pierpont, C. G. *J. Am. Chem. Soc.* **1986**, *108*, 7413. Haga, M.; Dodsworth, E. S.; Lever, A. B. P. *Inorg. Chem.* **1986**, *25*, 447. Auburn, P. R.; Dodsworth, E. S.; Haga, M.; Liu, W.; Nevin, W. A.; Lever, A. B. P. *Inorg. Chem.* **1991**, *30*, 3502. Lever, A. B. P.; Auburn, P. R.; Dodsworth, E. S.; Haga, M.; Nevin, W. A. *J. Am. Chem. Soc.* **1988**, *110*, 8076. Tse, Y.-H.; Auburn, P. R.; Lever, A. B. P. *Can. J. Chem.* **1992**, *70*, 1849. Metcalfe, R. A.; Dodsworth, E. S.; Fielder, S. S.; Stufkens, D. J.; Lever, A. B. P.; Pietro, W. J. *Inorg. Chem.* **1996**, *35*, 7741.

(5) Bhattacharya, S.; Pierpont, C. G. *Inorg. Chem.* **1994**, *33*, 6038. Vlček, A. *Comments Inorg. Chem.* **1994**, *16*, 207. Adams, D. M.; Dei, A.; Rheingold, A. L.; Hendrickson, D. N. *Angew. Chem., Int. Ed. Engl.* **1993**, *32*, 880. Jung, O. S.; Pierpont, C. G. *Inorg. Chem.* **1994**, *33*, 2227. Lange, C. W.; Conklin, B. J.; Pierpont, C. G. *Inorg. Chem.* **1994**, *33*, 1276. Pierpont, C. G.; Lange, C. W. *Prog. Inorg. Chem.* **1994**, *41*, 331. Benelli, C.; Dei, A.; Gatteschi, D.; Pardi, L. *Inorg. Chem.* **1990**, *29*, 3409. Bhattacharya, S.; Pierpont, C. G. *Inorg. Chem.* **1991**, *30*, 1511. Carugo, O.; Djinovic, K.; Rizzi, M.; Castellani, C. B. *J. Chem. Soc., Dalton Trans.* **1991**, 1255. Aratake, Y.; Koikawa, M.; Okawa, H.; Kida, S. *Inorg. Chim. Acta* **1991**, *190*, 85. Bag, N.; Pramanik, A.; Lahiri, G. K.; Chakravorty, A. *Inorg. Chem.* **1992**, *31*, 40. Bhattacharya, S.; Pierpont, C. G. *Inorg. Chem.* **1992**, *31*, 35. Hartl, F.; Vlcek, A. *Inorg. Chem.* **1992**, *31*, 2869. Shoner, S. C.; Bakac, A. *Inorg. Chem.* **1992**, *31*, 1001. Abakumov, G. A.; Cherkasov, V. K.; Bubnov, M. P.; Ellert, O. G.; Dobrokhotova, Z. V.; Zakharov, L. N. *Dokl. Akad. Nauk SSSR* **1993**, *328*, 332. Boone, S. R.; Pierpont, C. G. *Polyhedron* **1990**, *9*, 2267. Cohn, M. J.; Xie, C. L.; Tuchagues, J. P. M.; Pierpont, C. G.; Hendrickson, D. N. *Inorg. Chem.* **1992**, *31*, 5028. Ernst, S.; Haenel, P.; Jordanov, J.; Kaim, W.; Kasack, V.; Roth, E. *J. Am. Chem. Soc.* **1989**, *111*, 1733. Griffith, W. P. *Transition Met. Chem.* (*London*) **1993**, *18*, 250. Hartl, F.; Barbaro, P.; Bell, I. M.; Clark, R. J. H.; Snoeck, T. L.; Vlček, A., Jr. *Inorg. Chim. Acta* **1996**, *252*, 157.

(6) (a) Shin, Y. K.; Brunschwig, B. S.; Creutz, C.; Newton, M. D.; Sutin, N. *J. Phys. Chem.* **1996**, *100*, 1104 and references therein. (b) Lachance-Galang, K. J.; Doan, P. E.; Clarke, M. J.; Rao, U.; Yamano, A.; Hoffman, B. M. *J. Am. Chem. Soc.* **1995**, *117*, 3529. (c) Zhang, L. T.; Ondrechen, M. *Inorg. Chim. Acta* **1994**, *226*, 43.

(7) Lever, A. B. P. *Inorg. Chem.* **1990**, *29*, 1271.

S0020-1669(97)00236-X CCC: $14.00

further reduction to ruthenium(I) was not observed in these ammine species, nor did we observe a stable semiquinone complex.

The fully reduced $[Ru^{II}(NH_3)_4(R_2\text{-}CatH_4)]^{2+}$ species and the $[Ru^{II}(NH_3)_4(R_2\text{-}bqdi)]^{2+}$ and $[Ru^{III}(NH_3)_4(R_2\text{-}bqdi)]^{3+}$ series of complexes were studied, where R_2-bqdi = 4,5-disubstituted *o*-benzoquinone diimine with R = H, Cl, OCH_3. The

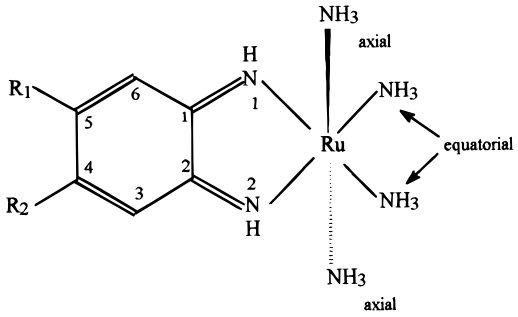

R_1= -H, Cl(1), -O(1)C(7)H_3

R_2= -H, Cl(2), -O(2)C(8)H_3

$[Ru^{II}(NH_3)_4(R_2\text{-}CatH_4)]^{2+}$ complexes were observed spectroelectrochemically, the $[Ru^{II}(NH_3)_4(R_2\text{-}QH_2)]^{2+}$ complexes were isolated as solids for all R, and $[Ru^{III}(NH_3)_4(H_2\text{-}QH_2)]^{3+}$ was generated by bulk electrolysis and was isolated as a solid. The electronic structure of these complexes is probed by electrochemistry, UV−vis, FTIR, and electron paramagnetic resonance (EPR) spectroscopies, and ZINDO molecular orbital calculations. The electronic properties of these complexes are shown to be a consequence of very extensive mixing between the metal dπ and quinonoid ligand π and π* orbitals. Because of the C_{2v} symmetry of these species, the relative mixing with π and with π* levels can be distinguished. The electronic spectra are assigned using the ZINDO calculations for support. Assignments for the Ru^{II} species follow accepted patterns, but the Ru^{III} species unexpectedly show significant MLCT as well as LMCT absorption.

Experimental Section

Reagents. All chemical products used were of reagent quality or better and were used as received, unless otherwise stated. Water was doubly distilled, the second time from potassium permanganate, and passed through Barnstead activated charcoal anion-exchange filters. All other solvents were distilled and dried by following literature methods.[8] *o*-Phenylenediamine (BDH) was recrystallized from benzene. 4,5-Dimethoxy-1,2-benzenediamine hydrochloride was synthesized according to a published procedure.[2]

Physical Measurements. Spectroscopic measurements were recorded on the following instruments: electronic spectra, Cary model 2400 spectrophotometer or Hewlett Packard 8452A diode array instrument; EPR spectra, Varian E4 electron spin resonance spectrophotometer (X band; 77 K glass in 3:2 toluene/acetonitrile); FTIR spectra, Unicam Mattson 3000 FTIR spectrometer as KBr pellets; NMR spectra, Bruker ARX-400, with dimethyl-d_6 sulfoxide as the solvent.

Electrochemical measurements were recorded using Princeton Applied Research Corp. model 173, 174, and 179 instruments or a Pine Instruments RDE-3 potentiostat. Results were obtained either using CH_3CN solutions containing 0.15 M tetrabutylammonium hexafluorophosphate, (TBA)PF_6, or using 0.1 M H_3PO_4 buffer solutions. Solutions typically contained 1×10^{-3} M of the complex. A platinum disk or a glassy carbon disk served as the working electrode, a platinum wire served as the counter electrode, and an SCE or AgCl/Ag wire was used as the reference electrode. Ferrocene was added as an internal standard when AgCl/Ag was used as the reference electrode, and potentials are reported vs SCE, assuming a ferrocenium/ferrocene potential of 0.425 V vs SCE with CH_3CN as the solvent.[9]

Spectroelectrochemical measurements were performed in an optically transparent thin-layer electrolytic (OTTLE) cell,[10] using a Princeton Applied Research Corp. model 174 potentiostat, with acetonitrile (0.3 M (TBA)PF_6 as the supporting electrolyte) or a 0.1 M H_3PO_4 buffer solution as the solvent. This cell uses transparent gold foil as the working and counter electrodes and an AgCl/Ag ribbon as the reference electrode. Bulk electrolysis was performed using a Hokuto-Denko Ltd. HA-310 potentiostat/galvanostat. The working electrode was platinum gauze, the counter was a graphite rod, and the reference was an AgCl/Ag wire. The reference and counter electrodes were each separated from the working electrode compartment by a glass frit. Argon gas was bubbled through the solution to mix it.

Calculations. INDO/1 and INDO/S calculations used the ZINDO program and a Hyperchem platform (Hypercube, Waterloo, Ontario, Canada). Data were processed on a Silicon Graphics Personal Iris Indigo R4000 or a Pentium 120 MHZ Intel computer running ZINDO/1 geometry optimizations and ZINDO/S spectroscopic and molecular orbital calculations.[11] Scaling parameters were $k_{p\sigma} = 1.267$ and $k_{p\pi} = 0.585$ together with the ruthenium bases of Krogh-Jespersen[12a] but with Ru β(4d) = −20 eV.[12b] Data concerning the geometries of the optimized structures are presented in the Supporting Information. There is general agreement between these distances and those anticipated from X-ray data of related materials.[13,14]

Syntheses. (a) $[Ru(NH_3)_4(4,5\text{-}R_2\text{-}bqdi)](CF_3SO_3)_2$ (R = H, Cl, OCH_3). The following general procedure was used to synthesize the bqdi complexes. *cis*-$[Ru(NH_3)_4(H_2O)_2](CF_3SO_3)_3$ (0.1 g, 0.15 mmol) was dissolved in methanol (5 mL). To this solution was added zinc amalgam (2.0 g), and the mixture was bubbled with argon for 15 min, during which the initial light yellow solution turned deep yellow, as Ru^{III} was reduced to Ru^{II}. The Ru^{II} complex was decanted under argon, and a deoxygenated solution of the appropriate *o*-phenylenediamine (0.15 mmol) was added to the solution of Ru^{II}. This mixture was stirred for 3 h, during which the initial yellow-orange solution changed to green, then to blue, and finally to orange. The orange color deepened when a drop of aqueous NH_3 was added, and the solution was bubbled with O_2 for 1 h. The volume was reduced until the product started to precipitate. The mixture was then cooled to −20 °C, and orange crystalline plates were formed. The crystals were filtered off, washed with melting methanol, ether, and hexane, and then air-dried. The yield can be increased by evaporating the mother liquor to dryness, dissolving the residue in the minimum amount of methanol, and finally cooling the solution to −20 °C. The resulting precipitate is then filtered off, washed with melting methanol, ether, and hexane, and then air-dried. Total yield: 80%.

Anal. Calcd for $[Ru(NH_3)_4(bqdi)](CF_3SO_3)_2$, $C_8H_{18}F_6N_6O_6RuS_2$: C, 16.75; H, 3.16; N, 14.65. Found: C, 16.68; H, 2.87; N, 14.54. Calcd

(8) Perrin, D. D.; Armarego, W. L. F.; Perrin, D. R. *Purification of Laboratory Chemicals*, 2nd ed.; Pergamon Press: Elmsford, New York, 1980.

(9) Gennett, T.; Milner, D. F.; Weaver, M. J. *J. Phys. Chem.* **1985**, *89*, 2787.

(10) Krejcik, M.; Danek, M.; Hartl, F. *J. Electroanal. Chem. Interfacial Electrochem.* **1991**, *317*, 179.

(11) Bacon, A. D.; Zerner, M. C. *Theor. Chim. Acta* **1979**, *53*, 21. Anderson, W. P.; Cundari, T.; Zerner, M. C. *Int. J. Quant. Chem.* **1991**, *39*, 31. Zerner, M. C. In *Metal-ligand Interactions*; Russo, N., Salahub, D. R., Eds.; Kluwer Academic Publishers: Dordrecht, The Netherlands, 1996; p 493. Anderson, W. P.; Cundari, T.; Drago, R. S.; Zerner, M. C. *Inorg. Chem.* **1989**, *29*, 1. Culberson, J. C.; Knappe, P.; Rösch, N.; Zerner, M. C. *Theor. Chim. Acta* **1987**, *71*, 21. Anderson, W. P.; Edwards, W. D.; Zerner, M. C. *Inorg. Chem.* **1986**, *25*, 2728. Zerner, M. C.; Loew, G. H.; Kirchner, R. F.; Mueller-Westerhoff, U. T. *J. Am. Chem. Soc.* **1980**, *102*, 589. Ridley, J.; Zerner, M. C. *Theor. Chim. Acta* **1973**, *32*, 111. Ridley, J.; Zerner, M. C. *Theor. Chim. Acta* **1976**, *42*, 223. Bacon, A. D.; Zerner, M. C. *Theor. Chim. Acta* **1979**, *53*, 21.

(12) (a) Krogh-Jespersen, K.; Westbrook, J. D.; Potenza, J. A.; Schugar, H. J. *J. Am. Chem. Soc.* **1987**, *109*, 7025. (b) Gorelsky, S. I.; Lever, A. B. P. Unpublished observation.

(13) Belser, P.; von Zelewsky, A.; Zehnder, M. *Inorg. Chem.* **1981**, *20*, 3098.

(14) Cheng, H. Y.; Peng, S. M. *Inorg. Chim. Acta* **1990**, *169*, 23.

Table 1. NMR Resonances (ppm) for $[Ru(NH_3)_4(4,5\text{-}R_2bqdi)](CF_3SO_3)_2$[a]

R = H	R = Cl	R = OMe	assignment
12.30 (s)	12.40 (s)	11.52 (s)	imine
7.44 (d)	7.85 (s)	6.84 (s)	bqdi ring
6.80 (d)			bqdi ring
4.32 (s)	4.49 (s)	4.00 (s)	equatorial NH_3
		3.72 (s)	methoxy CH_3
2.15 (s)	2.43 (s)[b]	1.90 (s)	axial NH_3

[a] Complexes in dimethyl-d_6 sulfoxide; s and d represent singlet and doublet. [b] Includes DMSO signal.

for $[Ru(NH_3)_4(4,5\text{-}Cl_2\text{-}bqdi)(CF_3SO_3)_2 \cdot 2H_2O$, $C_8H_{20}Cl_2F_6N_6O_8RuS_2$: C, 14.16; H, 2.97; N, 12.38. Found: C, 13.04; H, 2.35; N, 12.21. Calcd for $[Ru(NH_3)_4(4,5\text{-}(OCH_3)_2\text{-}bqdi)](CF_3SO_3)_2$, $C_{10}H_{22}F_6N_6O_8RuS_2$: C, 18.95; H, 3.50; N, 13.26. Found: C, 19.29; H, 3.48; N, 12.70.

(b) $[Ru(NH_3)_4(4,5\text{-}R_2\text{-}bqdi)]^{3+}$ (R = H, Cl, OCH_3). $[Ru(NH_3)_4(4,5\text{-}R_2\text{-}bqdi)](CF_3SO_3)_2$ (approximately 0.1 mmol) was dissolved in CH_3CN (4 mL) containing 0.1 M $(TBA)PF_6$ in a bulk electrolysis cell. The potential was polarized positive of the oxidation potential for the complex, and the solution was bubbled with N_2 for 3 h. During this time, the solution changed in color from orange to yellow. The electronic spectrum was monitored during the oxidation, and the polarization was stopped when the spectrum of the Ru^{III} complex was obtained, on the basis of the spectroelectrochemical results. The bulk electrolysis solution was used in order to obtain the EPR spectrum for the corresponding Ru^{III} species. A solid sample of $[Ru(NH_3)_4(bqdi)](PF_6)_3$ was isolated by removing the solvent from the bulk electrolysis solution and then washing the resulting solid with dichloromethane to remove the excess electrolyte, followed by washing with diethyl ether and hexane. This solid was stored in a vacuum desiccator. Anal. Calcd for $C_8H_{18}F_{18}N_6P_3Ru \cdot 2CH_2Cl_2$: C, 10.91; H, 2.51; N, 9.55. Found: C, 11.71; N, 2.31; N, 9.91.

Results and Discussion

NMR Spectroscopy. The NMR spectral data for the R_2-bqdi series of complexes are listed in Table 1. The characteristic proton resonances[1,15] for these complexes are those of (1) the imine protons which appear as a singlet, (2) the protons on the bqdi ring appearing as two doublets on the unsubstituted complex and a singlet for the substituted complexes, and (3) the protons of the coordinated ammines. The shifts which are observed in the proton resonances within this series of complexes can be attributed to the electron-donating/withdrawing ability of the substituent. The imine protons are shifted furthest upfield for the electron-donating methoxy substituent and furthest downfield for the electron-withdrawing chloride substituent. The NMR data provide additional unequivocal confirmation of the identities of these species.

The protons of the ammine groups which are in the same plane as the bqdi ligand (equatorial ammine groups) shift downfield relative to the protons of the axial ammine groups. The electron-withdrawing effect of the π-acceptor bqdi ligand will deshield these in-plane ammine protons.[16−22] The degree to which these protons are shifted is related to the electron-donating/withdrawing ability of the substituent, with the electron-withdrawing chloride substituent shifting the protons the furthest downfield and the electron-donating methoxy substituent shifting the protons the furthest upfield.

Electrochemistry. (See Figure S1.) (Note: Figure and table numbers preceded by "S" refer to material in the Supporting Information.) The oxidation of these complexes in acetonitrile, is a chemically reversible process and the potential of the corresponding anodic wave is dependent on the substituent on the QH_2 ligand; see Table 2. Given that the bulk solution is already at the quinone oxidation level and taking note of the ligand electrochemical parameters[7] for ammonia (0.07) and bqdi (ca. 0.28),[1,22] the anodic step is clearly assigned to the $Ru^{III/II}$ couple. The shifts in this oxidation potential are a reflection of the donor/acceptor ability of the substituents, with the electron-donating methoxy substituent shifting the $Ru^{III/II}$ oxidation to less positive potentials and the electron-withdrawing chloride substituent shifting the $Ru^{III/II}$ couple to more positive potentials, relative to the unsubstituted complex. Estimates of the $E_L(L)$ parameters for the substituted bqdi species are also given in Table 2.

The reduction of these complexes is more complicated than the oxidation. The $[Ru(bpy)_2(R_2\text{-}bqdi)]^{2+}$ complexes typically show several reduction processes,[1,5] namely the conversion of the quinonoid (QH_2) form to the semiquinonoid (SqH_2) form and the conversion of the semiquinonoid form to the diamido ($CatH_2$) or *o*-phenylenediamine ($CatH_4$) forms. This is not seen for the tetraammine complexes. Initially what appears to be a reversible one-electron wave is observed; however, continued cycling around this redox couple results in a gradual loss of current, until the electrode is completely passivated. After polishing of the electrode, the original cyclic voltammogram is regenerated. Therefore, it is likely that the reduction of these complexes results in the formation of an insulating deposit on the electrode surface. The semiquinonoid species which is produced in this reduction step is probably very reactive and may react with traces of water or with the solvent in order to form the deposit.

Although the reduction processes are irreversible, the first scan represents the reduction potential of these species, presumably to the semiquinonoid form. The oxidation potentials are linearly dependent on the reduction potentials, giving a regression coefficient, R^2, of 0.99, suggesting that any kinetic or coupled chemical reaction contributions to these reduction processes are probably similar in the three species and that comparisons between them is meaningful even though the processes are irreversible.[23−26] The shift in reduction potential from R = Cl to R = OCH_3 is quite large (490 mV), showing that the substituents have a significant influence on the net electron density at the coordinated ligand site.

When 0.1 M H_3PO_4 is used as the solvent (Figure S1), there is a proton source available for the reduced complexes providing a different reduction pathway, with the final product being the ($CatH_4$) *o*-phenylenediamine complex. The electrochemical data for the $[Ru(NH_3)_4(R_2\text{-}QH_2)]^{2+}$ complexes in various aqueous phosphate buffer solutions are listed in Table 2. Oxidation of the metal center is appreciably easier (less positive potential) in aqueous medium than in CH_3CN, probably because the increased polarity of the aqueous solvent stabilizes the more highly charged Ru^{III} species better than CH_3CN.

(15) Masui, H. Ph.D. Thesis, York University, Ontario, Canada, 1994.
(16) Metcalfe, R. A.; Vasconcellos, L. C. G.; Franco, D. W.; Lever, A. B. P. Manuscript in preparation.
(17) Foust, R. D.; Ford, P. C. *J. Am. Chem. Soc.* **1972**, *94*, 5686.
(18) Stein, C. A.; Taube, H. *J. Am. Chem. Soc.* **1978**, *100*, 336.
(19) Joss, S.; Reust, H.; Ludi, A. *J. Am. Chem. Soc.* **1981**, *103*, 981.
(20) Evans, I. P.; Everett, G. W.; Sargeson, A. M. *J. Am. Chem. Soc.* **1976**, *98*, 8041.
(21) Lehmann, H.; Schenk, K. J.; Chapuis, G.; Ludi, A. *J. Am. Chem. Soc.* **1979**, *101*, 6197.
(22) Ebadi, M.; Lever, A. B. P. Paper in preparation.
(23) Dodsworth, E. S.; Vlček, A. A.; Lever, A. B. P. *Inorg. Chem.* **1994**, *33*, 1045.
(24) Hupp, J. T.; Meyer, T. J. *Inorg. Chem.* **1987**, *26*, 2332.
(25) Ross, H. B.; Boldajii, M.; Rillema, D. P.; Blanton, C. B.; White, R. P. *Inorg. Chem.* **1989**, *28*, 1013.
(26) Lever, A. B. P.; Dodsworth, E. S. In *Inorganic Electronic Structure and Spectroscopy*; Solomon, E. I., Lever, A. B. P., Eds.; J. Wiley and Sons: New York, 1998; Vol. 2.

Table 2. Electrochemical Data for the $[Ru(NH_3)_4(R_2\text{-bqdi})]^{2+}$ Complexes

R	solvent	$Ru^{III/II}QH_2$ potential (mV) vs SCE	reoxidation[a] potential (mV) vs SCE	reduction potential (mV) (irreversible) vs SCE	ΔE(redox) (mV)	$E_L(R_2\text{-bqdi})$
H	CH_3CN[b]	860		−870[d]	1730	0.41
H	0.1 M H_3PO_4[c]	540	259, 10	−860[f]	1400	*e*
H	0.1 M KH_2PO_4[g]	540	80, −140	−860[f]	1400	
Cl	CH_3CN[b]	990		−660[d]	1650	0.47_5
Cl	H_3PO_4[c]	650	300	−730[f]	1380	*e*
OCH_3	CH_3CN[b]	600		−1150[d]	1750	0.28
OCH_3	0.1 M H_3PO_4[c]	320	70	−400[f]	720	*e*
OCH_3	0.1 M KH_2PO_4[g]	310	−160, −340	−940[f]	1250	
OCH_3	0.1 M K_2HPO_4[h]	260	−370, −480	−930[f]	1190	

[a] Irreversible, multiple-wave reoxidation of $CatH_4$ to QH_2—see refs 16 and 27. [b] 0.15 M (TBA)PF_6, CH_3CN. [c] pH = 1.6. [d] QH_2/SqH_2 process. [e] Because of solvation effects, one cannot derive a reliable value of $E_L(R_2\text{-bqdi})$ from the aqueous data. [f] 2-electron/2-proton coupled reactions corresponding to the $QH_2/CatH_4$ process. [g] pH = 4.4 [h] pH = 8.7.

The reduction of the $[Ru(NH_3)_4(R_2\text{-bqdi})]^{2+}$ complex to the $[Ru^{II}(NH_3)_4(R_2\text{-}CatH_4)]^{2+}$ complex followed by the reoxidation to the $[Ru(NH_3)_4(R_2\text{-bqdi})]^{2+}$ complex is a complicated process that is discussed in more detail elsewhere.[27] Electrochemical parameter theory[7] leaves little doubt that the first step in the oxidation of $[Ru^{II}(NH_3)_4(CatH_4)]^{2+}$ must be formation of $[Ru^{III}(NH_3)_4(CatH_4)]^{3+}$. EPR evidence for the formation of the ruthenium(III) intermediate species is presented for an analogous system elsewhere.[16]

Electronic Spectroscopy and Spectroelectrochemistry. The electronic spectroscopic data for the three Ru^{II} complexes of the substituted bqdi complexes are shown in Table 3. Aspects of the electronic structure of the analogous $[Ru(bpy)_2(bqdi)]^{2+}$ complexes with these ligands were previously discussed by Masui.[1] A summary of comparative electrochemical and spectroscopic data for the $[Ru(NH_3)_4(bqdi)]^{2+}$ and the $[Ru(bpy)_2(bqdi)]^{2+}$ complexes is presented in Table 4. The oxidation potentials of the bis(bipyridine) complexes are much more positive[1] than those of the tetraammine complexes (Table 2), consistent with the greater electron richness of the tetraammine ligands compared with the bis(bipyridine) fragment. In terms of electronic spectra, this should translate to lower energy MLCT transitions[28] for the tetraammine complexes than for the bis(bipyridine) complexes. Indeed, this is true for the lowest energy very weak near-infrared band, ν_1, which has MLCT character, as discussed in depth below. However, it is not true for the prominent visible-region absorption band, ν_2. In the tetraammine $Ru^{II}QH_2$ oxidation state, this strong band, ν_2, appears in the range 20 080−21 280 cm^{-1} and is associated with the Ru^{II} (d) → QH_2 (π^*) MLCT transition.[1−4] Thus the energy of this MLCT transition is observed at a higher energy in the tetraammine complexes than in the bis(bipyridine) complexes. There are also higher energy $\pi \rightarrow \pi^*$ bands.

The reversible spectroscopic changes which occur when the $[Ru^{II}(NH_3)_4(R_2\text{-bqdi})]^{2+}$ complexes are oxidized, in 0.1 M H_3PO_4, are shown in Figures 1 and S2. Upon oxidation to Ru^{III}, there are a loss of the Ru^{II} (d) → QH_2 (π^*) MLCT transition and the growth of an intense, narrow transition near 24 000 cm^{-1}. There is also a substantial blue shift of the lowest energy $\pi \rightarrow \pi^*$ transition of some 7000 cm^{-1}, and two new transitions appear near 20 600 cm^{-1} and at 30 900 cm^{-1}. These various transitions are discussed in more depth after consideration, below, of the ZINDO analysis.

As anticipated from the cyclic voltammetric results, the spectroelectrochemical reduction of $[Ru^{II}(NH_3)_4(R_2\text{-bqdi})]^{2+}$ in CH_3CN results in the irreversible loss of absorbance of the Ru (d) → QH_2 (π^*) transition, with no isosbestic points and no spectroscopic evidence for the existence of a semiquinonoid intermediate; therefore, CH_3CN was discarded as the solvent for reduction.

The reduction of the complexes, however, can be cleanly observed when 0.1 M H_3PO_4 is used as the solvent. The resulting spectroscopic changes can be seen in Figures 1 and S3. As the complex is reduced, the Ru (d) → QH_2 (π^*) MLCT transition diminishes in intensity, until it completely disappears. The process being observed is the reduction of the R_2-bqdi ligand to the fully reduced $[Ru(NH_3)_4(R_2\text{-}CatH_4)]^{2+}$ species. This process can be reversed under acidic conditions, regenerating the $[Ru^{II}(NH_3)_4(R_2\text{-}QH_2)]^{2+}$ species. The lack of any significant visible-region absorption for the $[Ru(NH_3)_4(R_2\text{-}CatH_4)]^{2+}$ species provides confirmatory spectroscopic evidence for its formulation, since this species would possess no low-energy charge transfer bands. As in CH_3CN, there was no spectroscopic evidence for the formation of any semiquinonoid intermediates.

Electron Paramagnetic Resonance Spectroscopy. Bulk electrolysis of the Ru^{II} complexes at potentials positive of their $Ru^{III/II}$ redox couple results in the formation of the corresponding Ru^{III} complexes. The EPR spectra for these complexes were recorded in a solvent mixture of 2:3 CH_3CN/toluene at liquid-N_2 temperatures and are shown in Figure S4. The spectra are typical for a rhombically distorted, low-spin d^5 Ru^{III} species.[6,29−33] The unsubstituted complex has $g_1 = 2.69$, $g_2 = 2.42$, and $g_3 = 1.72$, the dichloro complex has $g_1 = 2.71$, $g_2 = 2.39$, and $g_3 = 1.73$, and the dimethoxy complex has g_1 and g_2 overlapping between 2.63 and 2.53 and $g_3 = 1.67$. The spectra show that the magnitudes of the three g values are sensitive to the substituent on the bqdi ring, with the greatest change being seen in the overlap of g_1 and g_2 for the dimethoxy complex. These data provide unequivocal evidence that the first oxidation couple generates a species in which the unpaired electron resides in an orbital which has significant ruthenium character.

(27) Metcalfe, R. A.; Lever, A. B. P. To be published.
(28) Lever, A. B. P. *Inorganic Electronic Spectroscopy*, 2nd ed.; Elsevier: Amsterdam, 1984.
(29) Rieger, P. H. *Coord. Chem. Rev.* **1994**, *135/136*, 203 and references therein.
(30) (a) Chakravarty, A. R.; Chakravorty, A. *Inorg. Chem.* **1981**, *20*, 3138. (b) Bag, N.; Lahiri, G. K.; Chakravorty, A. *J. Chem. Soc., Dalton Trans.* **1990**, 1557. (c) Lahiri, G. K.; Bhattacharya, S.; Mukherjee, M.; Mukherjee, A. K.; Chakravorty, A. *Inorg. Chem.* **1987**, *26*, 3359. (d) Lahiri, G. K.; Bhattacharya, S.; Ghosh, B. K.; Chakravorty, A. *Inorg. Chem.* **1987**, *26*, 4324.
(31) Gupta, H. K.; Dikshit, S. K. *Polyhedron* **1987**, *6*, 1009. Hush, N. S.; Edgar, A. *Chem. Phys. Lett.* **1980**, *69*, 128. Matsumoto, K.; Matsumoto, T.; Kawano, M.; Ohnuki, H.; Shichi, Y.; Nishide, T.; Sato, T. *J. Am. Chem. Soc.* **1996**, *118*, 3597.
(32) Kaplan, D.; Navon, G. *J. Phys. Chem.* **1974**, *78*, 700. Kasack, V.; Kaim, W.; Binder, H.; Jordanov, J.; Roth, E. *Inorg. Chem.* **1995**, *34*, 1924.
(33) DeSimone, R. E.; Drago, R. S. *J. Am. Chem. Soc.* **1970**, *92*, 2343. Sakai, S.; Yanase, Y.; Hagiwara, N.; Takeshita, T.; Naganuma, H.; Ohyoshi, A.; Ohkubo, K. *J. Phys. Chem.* **1982**, *86*, 1038.

Table 3. Experimental and Calculated Electronic Spectral Data for the $[Ru(NH_3)_4(R_2\text{-BQDI})]^{2+/3+}$ Series of Complexes and Related Complexes[a]

(a) Ruthenium(II) Species

	transition			
	$3a_2 \rightarrow 4b_2$	$3b_2 \rightarrow 4b_2$	$3a_2 \rightarrow 4a_2$	$2b_2 \rightarrow 4b_2$
	(i) $[Ru(NH_3)_4(bqdi)]^{2+}$ [HOMO = #39, $3a_2$]			
exptl energy[b] (cm^{-1})	10 360 ν_1	21 280 ν_2 (4.01, 3610, 0.17)	38 760 (3.99, 4990, 0.22)	51 020
calcd energy[c] (cm^{-1})	11 580 (0.01)	23 050 (0.48)	38 970 (0.53)	47 000 (0.16)
assignment	#39 → #40	#38 → #40	#39 → #41	#35 → #40
	$(d_{xz} - \pi) \rightarrow (\pi^* - d_{yz})$	$(d_{yz} + \pi^*) \rightarrow (\pi^* - d_{yz})$	$(d_{xz} - \pi) \rightarrow \pi^*$	$\pi \rightarrow \pi^*$
	(ii) $[Ru(NH_3)_4(4,5\text{-}Cl_2\text{-bqdi})]^{2+}$ [HOMO = #45, $3a_2$]			
exptl energy[b] (cm^{-1})	9700 ν_1	20 920 ν_2 (4.05, 3260, 0.17)	36 500 (3.99, 5540, 0.25)	47 620
calcd energy[c] (cm^{-1})	11 530 (0.01)	21 520 (0.49)	38 100 (0.31)	41 600 (0.54)
assignment	#45 → #46	#44 → #46	#45 → #47	#41 → #46
	$(d_{xz} - \pi) \rightarrow (\pi^* - d_{yz})$	$(d_{yz} + \pi^*) \rightarrow (\pi^* - d_{yz})$	$(d_{xz} - \pi) \rightarrow \pi^*$	$\pi \rightarrow \pi^*$
	(iii) $[Ru(NH_3)_4(4,5\text{-}(OCH_3)_2\text{-bqdi})]^{2+}$ [HOMO = #51, $3a_2$]			
exptl energy[b] (cm^{-1})	11 200, 13 870 ν_1	20 080 ν_2 (4.00, 3400, 0.16)	38 460 (4.03, 6520, 0.32)	50 000[d]
calcd energy[c] (cm^{-1})	12 425 (0.01)	20 390 (0.56)	38 320 (0.78)	47 800 (0.31)
assignment	#51 → #52	#50 → #52	#51 → #53	#50 → #54
	$(d_{xz} - \pi) \rightarrow (\pi^* - d_{yz})$	$(d_{yz} + \pi^*) \rightarrow (\pi^* - d_{yz})$	$(d_{xz} - \pi) \rightarrow \pi^*$	$3b_2 \rightarrow 5b_2$
				#48 → #53
				$2a_2 \rightarrow 4a_2$
				$(d, \pi) \rightarrow \pi^*$

(b) Ruthenium(III) Species

exptl energy[b] (cm^{-1})	assignment	calcd energy[c] (cm^{-1})
	(i) $[Ru(NH_3)_4(bqdi)]^{3+}$ (SOMO = #39, $3a_2$)	
45 450	$\pi \rightarrow (\pi^* - d)$, LMCT	42 000 (0.28)
	#35 → #40; $2b_2 \rightarrow 4b_2$	
	#32 → #39; $1a_2 \rightarrow 3a_2$	
30 860	$\pi \rightarrow (\pi^* - d)$, LMCT	36 450 (0.23)
	#32 → #39; $1a_2 \rightarrow 3a_2$	
24 040 (4.08, 1740, 0.1)	$(d,\pi) \rightarrow (\pi^* - d)$	28 140 (0.45)
	#35,38 → #40; $2b_2$,$3b_2 \rightarrow 4b_2$	
20 120 (3.17, 2000, 0.01)	$(d,\pi) \rightarrow (\pi^* - d)$	27 000 (0.16)
	#35,38 → #40; $2b_2$,$3b_2 \rightarrow 4b_2$	
	#37,39 → #41; $2a_2$,$3a_2 \rightarrow 4a_2$	
12 500	$(d + \pi) \rightarrow (\pi^* - d)$	13 700 (0.03)
	#39 → #40; $3a_2 \rightarrow 4b_2$	
	#37 → #40; $2a_2 \rightarrow 4b_2$	
	(ii) $[Ru(NH_3)_4(4,5\text{-}Cl_2\text{-bqdi})]^{3+}$ [SOMO = #45, $3a_2$]	
41 670	$(d,\pi) \rightarrow \pi^*$, LMCT, MLCT	43 730 (0.16)
	#36 → #45; $1a_2 \rightarrow 3a_2$	40 940 (0.46)
	#43,45 → #47; $2a_2$,$3a_2 \rightarrow 4a_2$	
29 590	$(d,\pi) \rightarrow (\pi^* - d)$, LMCT	34 850 (0.19)
	#41 → #46; $2b_2 \rightarrow 4b_2$	
	#36 → #45; $1a_2 \rightarrow 3a_2$	
23 580 (4.15, 2000, 0.13)	$(d,\pi) \rightarrow (\pi^* - d)$, MLCT	27 050 (0.74)
	#44 → #46; $3b_2 \rightarrow 4b_2$	
	#41 → #46; $2b_2 \rightarrow 4b_2$	
19 610[d] (3.12, 2250, 0.01)	$(d,\pi) \rightarrow (\pi^* - d)$, MLCT	14 120 (0.02)
	#45 → #46; $3a_2 \rightarrow 4b_2$	
	#43 → #46; $2a_2 \rightarrow 4b_2$	
	(iii) $[Ru(NH_3)_4(4,5\text{-}(OCH_3)_2\text{-bqdi})]^{3+}$ [SOMO = #51, $3a_2$]	
43 100	$\pi \rightarrow \pi^*$	
31 060	?	25 900? (0.09)
23 470 (4.15, 2000, 0.13)	#50 → #52; $3b_2 \rightarrow 4b_2$ (MLCT)	22 520 (0.24)
	#48 → #51; $2a_2 \rightarrow 3a_2$ (LMCT)	
19 100 (2.89, 2960, 0.01)	?	21 070 (0.02)
not obsd	#50 → #52; $3b_2 \rightarrow 4b_2$ (MLCT)	11 380 (0.003)
	#48 → #51; $2a_2 \rightarrow 3a_2$ (LMCT)	

(c) $[Ru(bpy)_2(bqdi)]^{2+}$ [HOMO = #81][e]

exptl energy[b] (cm^{-1})	assignment	calcd energy[c] (cm^{-1})
35 650	$\pi \rightarrow \pi^*$ bpy	
30 850	Ru → π^* (2) bpy; #81 → #86	31 960 (0.14)
22 450	Ru → π^* (1) bpy; #80 → #83	23 920 (0.14)
19 400 (4.24, 2850)	$(d_{yz} + \pi^*) \rightarrow (\pi^* - d_{yz})$; #79 → #82	19 700 (0.57)
13 250	#80 → #82	11 150 (0.003)
	#81 → #82	9 700 (0.004)

[a] All data were collected in 0.1 M H_3PO_4 except where noted. [b] Data in parentheses are log ϵ, half-bandwidth, and oscillator strength. [c] Values in parentheses are the oscillator strengths. [d] Tentative assignment. [e] Data collected in CH_3CN.

Table 4. Comparison of Spectroscopic and Electrochemical Data for $[Ru(NH_3)_4(bqdi)]^{2+}$ with Spectroscopic and Electrochemical Data[1] for $[Ru(bpy)_2(bqdi)]^{2+}$ [a] (Data vs SCE)

property	$[Ru(NH_3)_4(bqdi)]^{2+}$	$[Ru(bpy)_2(bqdi)]^{2+}$
$E(Ru^{III/II})$	0.86 V (0.41 V)[b]	1.35 V (0.28 V)[b]
$E(L/L^-)$[c]	−0.87 V	−0.47 V
$E(\nu_2)$[d]	21 140 cm^{-1} ($C(\nu_2) = 7200\ cm^{-1}$)[e]	19 400 cm^{-1} ($C(\nu_2) = 4700\ cm^{-1}$)[e]
f, $\Delta_{1/2}$[f]	0.16, 3230 cm^{-1}	0.26, 2580 cm^{-1} ($(d_{yz} + \pi^*) \rightarrow (\pi^* - d_{yz})$)
$E(\nu_1)$[g]	10 360 cm^{-1} ($C(\nu_1) = -3600\ cm^{-1}$)[h]	13 250 cm^{-1} ($C(\nu_1) = -1400\ cm^{-1}$)[h]

[a] Spectroscopic data were recorded in CH_3CN; electrochemical data were recorded in CH_3CN containing 0.1 M $(TBA)PF_6$. [b] Calculated E_L(bqdi). [c] First reduction potential localized primarily at bqdi. [d] Energy of principal visible-region band. [e] Value of C for ν_2 in eq 1. [f] f = oscillator strength; $\Delta_{1/2}$ = half-bandwidth. [g] Near-infrared-region weak absorption, ν_1, corresponding to the HOMO → LUMO transition. [h] The value of C for ν_1 in eq 1.

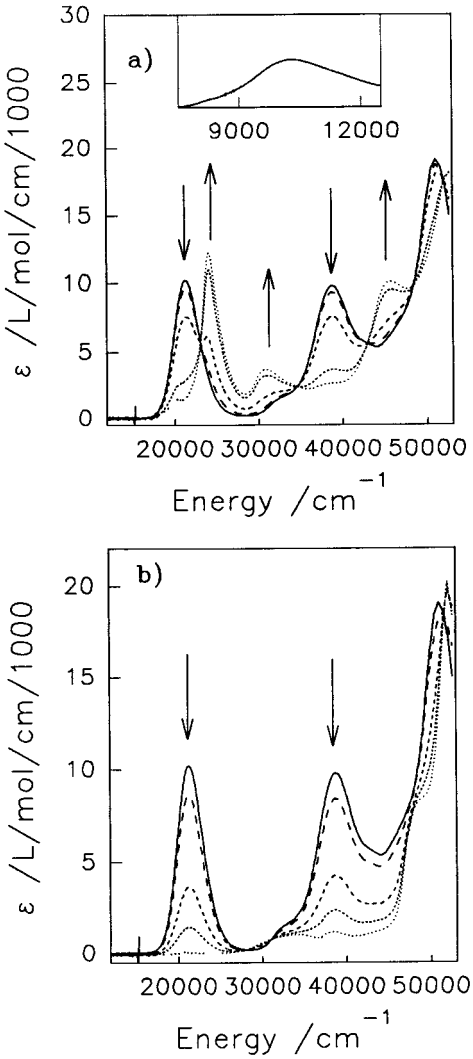

Figure 1. (a) Spectroelectrochemical oxidation of a 0.25 M solution of $[Ru(NH_3)_4(bqdi)]^{2+}$ (solid line), in 0.1 M H_3PO_4, forming $[Ru(NH_3)_4(bqdi)]^{3+}$ (···). (b) Spectroelectrochemical reduction of a 0.25 M solution of $[Ru(NH_3)_4(bqdi)]^{2+}$ (solid line) in 0.1 M H_3PO_4, forming $[Ru(NH_3)_4(catH_4)]^{2+}$ (···). Multiple spectra show the time dependence as the reaction proceeds. The insert shows the near-infrared region and the $3a_2 \rightarrow 4b_2$ (ν_1) transition for $[Ru(NH_3)_4[bqdi)]^{2+}$.

Electronic Structures of the bqdi Complexes—ZINDO Calculations. (a) Free Ligand. We choose a frame of reference where the bqdi plane is *xz* and the *z* axis bisects the RuNCCN metallacycle. Although the free diimine ligand does not exist, one can compute (ZINDO/S) its frontier orbitals, revealing the pattern shown in Figure 2. It has C_{2v} symmetry as do the metal complexes if one disregards lower symmetry orientations of the N−H bonds. In the free ligand, there are four a_2 and four b_2 orbitals of π or π^* character. There are also σ or σ^* levels of a_1 or b_1 symmetry. Thus the metal d_{xy} and d_{yz} orbitals can couple to the ligand π or π^* orbitals, while the metal d_{xz} orbitals will have σ symmetry. However note that the pair of axial ammonia ligands generate a σ-SALC (SALC = symmetry adapted linear combination) ($\sigma_1 - \sigma_2$) of b_2 symmetry and this interacts strongly with the lowest lying bqdi b_2 (π) orbital, generating what we will describe as $1b_{2s}$ and $1b_{2a}$ for the symmetric and antisymmetric combinations, respectively.

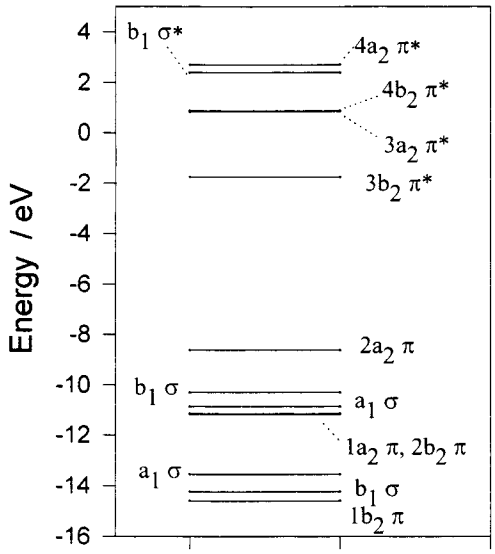

Figure 2. ZINDO/S-calculated frontier orbitals for the free ligand bqdi. The nuclear coordinates in $[Ru(NH_3)_4(bqdi)]^{2+}$ were used with the ruthenium ammine fragment deleted.

Further, the R = Cl, OMe substituted species generate an additional a_2 set and an additional b_2 set of orbitals which couple to the ring a_2 and b_2 orbitals. We wish to retain a rational numbering scheme such that comparisons can readily be made over all three series of complexes, i.e. so that the mixing in a specific orbital in one complex can be readily compared with the corresponding orbital in another complex. Therefore, these additional a_2 and b_2 orbitals are subsumed into $1a_2$ and $1b_2$. In the former case, this generates the labels $1a_{2s}$ and $1a_{2a}$. Thus all the +2 and +3 species have $3a_2$ as their HOMO and SOMO, respectively. There are now three $1b_2$ orbital labels for R = Cl, OMe, retaining then $4b_2$ as the LUMO in all the complexes.

(b) Ruthenium(II) Species. Recent ZINDO treatments of ruthenium species have shown that this method is successful in predicting their mixing behavior and spectroscopic properties.[6a,34] We therefore have some confidence that the method is meaningful. For example, our[35] ZINDO analysis of tris(bipyridine)-ruthenium(II) yields mixing data very similar to those recently reported[36] for this archetypical molecule, using density functional theory.

(34) (a) Ward, M. D. *Inorg. Chem.* **1996**, *35*, 1712. (b) Lewis, N. A.; Pan, W. *Inorg. Chem.* **1995**, *34*, 2244.
(35) Gorelsky, S. I.; Dodsworth, E. S.; Vlček, A. A.; Lever, A. B. P. Paper in preparation.

ZINDO/1 optimization of $[Ru(NH_3)_4(bqdi)]^{2+}$ and its substituted analogues gave structures with $Ru-NH_3$ bond distances close to 200 pm rather than values around 215 pm observed with pentaammineruthenium(II) species.[37] Thus the optimization was repeated after constraining the Ru−N distances to be $Ru-NH_3(ax) = 216.6$ and $Ru-NH_3(eq) = 214$ pm, on the basis of pentammineruthenium(II) crystal structures.[37] ZINDO/1 did approximately reproduce the anticipated distances for the Ru−N(bqdi) and internal bqdi and bpy C═C and C═N bonds, including the C−C distance alternation expected for the quinonoid ligand. The R = OMe species optimized with the $C_{bqdi}-O-C_{CH_3}$ angle at about 114° and with the plane of these three atoms lying in the bqdi plane with the methyl groups pointing outward. This is consistent with previous X-ray data for *o*-dimethoxybenzene species[38] and retains the C_{2v} symmetry of the molecule. Indeed, one can be fairly certain that the C_{2v} symmetry is retained experimentally, because the electronic spectrum of the R = OMe species is very similar to those of R = H, Cl. ZINDO/S predicts a very much more complex spectrum if the C_2 axis in the R = OMe species had been lost. These optimizations were followed by ZINDO/S derivations of the electronic spectra of these species using 800 singly excited transitions (SECI) from the top 20 populated levels to the first 20 unpopulated levels, to generate the configurational interaction (CI) matrix.

We consider the metal−ligand mixing reported by the ZINDO/S analysis which leads to a fairly accurate prediction of the electronic spectrum. The metal d_{xy} (a_2) and d_{yz} (b_2) orbitals couple with ligand a_2 and b_2 orbitals, generating a total of five a_2 and six b_2 orbitals (including the σ-b_2 on the axial NH_3 and subject to the modifications discussed immediately above for R = Cl, OMe), with the degree of mixing shown in Table 5 and with molecular orbital energies reported in Tables S1−S6 and for R = H in Figure 3. The HOMO is $3a_2$ and the LUMO $4b_2$.

There is extensive mixing in $2a_2$ ($\pi + d_{xz}$) and $3a_2$ ($d_{xz} - \pi$) (HOMO), but $1a_2$ shows less mixing (than $2a_2$ and $3a_2$), while $4a_2$ (π^*) and especially $5a_2$ (π^*) remain predominantly ligand-localized probably because these orbitals are more energetically removed from the d_{xz} orbital. The absence of mixing in the $4a_2$, $5a_2$ (π^*) orbitals signifies that the mixing with d_{xy} (a_2) comes exclusively from bqdi (π) with essentially no bqdi (π^*) component. This extensive $d_{xy} \leftrightarrow \pi$ mixing in the a_2 orbitals is an aspect often neglected in Ru^{II} chemistry but recognized recently by others.[6]

Thus, mixing with the π^* orbitals is determined by the b_2 symmetry matrices. The high-energy $5b_2$ is a pure ligand orbital, but the LUMO, $4b_2$, shows extensive π^*-d mixing, being evidence that π back-donation is important in these systems. Approximately 0.4e is back-donated into $4b_2$. Orbital $3b_2$ ($d + \pi,\pi^*$) is mostly metal-localized but does have significant ligand character. This is the orbital which is supposedly stabilized by the π-back-donation mechanism, but it lies at HOMO-1 not HOMO-2 as might have been inferred from a Magnuson and Taube model[39] because it is destabilized by interaction (coupling) with the lower lying $2b_2$ orbital. Orbitals $1b_{2s}$, $1b_{2a}$, and $2b_2$, while lying fairly far removed from the d_{yz} orbital, still have some metal content. These overall features are shown by all three species, R = H, Cl, and OCH_3, with only relatively small variations.

Table 5. Summary of Percentage Ruthenium, Benzoquinone Diimine, and Ammonia Contributions to the Frontier Orbitals[a] of $[Ru(NH_3)_4(bqdi)]^{2+}$, $[Ru(NH_3)_4(bqdi)]^{3+}$, and $[Ru(bpy)_2(bqdi)]^{2+}$ [b]

(a) $[Ru(NH_3)_4(bqdi)]^{2+}$

MO	% Ru	% bqdi	% NH_3
$1b_{2s}(NH_3)$[c]	7	53	40 [27]
$1b_{2a}(NH_3)$[c]	5	38	57 [30]
$1a_2$	9	88	3 [33]
$2b_2$	11	85	4 [35]
$2a_2$	28	71	1 [36]
$3b_2$	61	37	2 [38]
$3a_2$ (HOMO)	58	41	1 [39]
$4b_2$ (LUMO)	20	79	1 [40]
$4a_2$	1	99	0 [41]
$5b_2$	0.5	99	0.5 [43]
$5a_2$	0	100	0 [47]

(b) $[Ru(NH_3)_4(bqdi)]^{3+}$

MO	% Ru	% bqdi	% NH_3
$1b_{2s}(NH_3)$[c]	5	61	34 [27]
$1b_{2a}(NH_3)$[c]	5	31	65 [30]
$1a_2$	9	89	2 [32]
$2b_2$	14	82	4 [35]
$2a_2$	30	68	2 [37]
$3b_2$	65	32	3 [38]
$3a_2$ (SOMO)	55	43	2 [39]
$4b_2$ (LUMO)	12	87	1 [40]
$4a_2$	1	99	0 [41]
$5b_2$	0	100	0 [42]
$5a_2$	0	100	0 [47]

(c) $[Ru(bpy)_2(bqdi)]^{2+}$

MO	% Ru	% bqdi	% bpy
HOMO	70	21	9 [81]
LUMO	18	74	8 [82]

[a] The orbital index is cited in square brackets. Only orbitals of π symmetry are shown. A more complete listing with the intervening σ levels is shown in the Supporting Information. Note: for simplicity, to enable these totals to be 100%, the ruthenium contribution is the total 4d, 5s, and 5p contributions. However the 5s and 5p contributions are mostly very small. [b] The data for the R = Cl and R = OCH_3 species are given in the Supporting Information. [c] Symmetric, $1b_{2s}$, and antisymmetric, $1b_{2a}$, coupling of the bqdi $1b_2$ orbital with the b_2 $\sigma(NH_3)$ orbital. Data for the other species are presented in the Supporting Information.

The percentage Ru contribution residing in each orbital is noted. With no mixing, each d orbital would reside 100% on ruthenium, i.e. 200% in the dπ orbitals a_2 and b_2. Given the high symmetry of these molecules, the total d orbital contribution to the set of na_2 and nb_2 orbitals distributed over the entire molecule must also be 200%. Thus, the extent of π mixing may be estimated first by considering the total Ru contribution to the $3b_2$ and $3a_2$ orbitals plus the π-back-bonding contribution in $4b_2$. This is seen, for the Ru^{II} species (Table 5), to be 139, 148, and 141% for R = H, Cl, and OMe, respectively. With pure d orbitals and no mixing, these numbers would all sum to 200%. Thus the differences from 200%, namely 61, 52, and 59%, respectively, reflect the extent of π mixing. While these numbers may not be highly accurate since they will, inter alia, depend upon how good the theory and geometry optimization are, it is gratifying that the trend is as would be expected, with the electron-withdrawing Cl substituents rendering the R = Cl species the poorest π-mixing ligand.

The HOMO and LUMO energies for the three Ru^{II} species correlate linearly with the $Ru^{III/II}$ and first reduction potentials, respectively (Figure S5), recorded in acetonitrile. Here we merely comment that this correlation exists. Such a correlation[40]

(36) Daul, C.; Baerends, E. J.; Vernooijs, P. *Inorg. Chem.* **1994**, *33*, 3538.
(37) Gress, M. E.; Creutz, C.; Quicksall, C. O. *Inorg. Chem.* **1981**, *20*, 1522. Stynes, H. C.; Ibers, J. A. *Inorg. Chem.* **1971**, *10*, 2304. Krogh-Jespersen, K.; Zhang, X.; Ding, Y.; Westbrook, J. D.; Potenza, J. A.; Schugar, H. J. *J. Am. Chem. Soc.* **1992**, *114*, 4345.
(38) Diederich, F.; Jonas, U.; Gramlich, V.; Herrmann, A.; Ringsdorf, H.; Thilgen, C. *Helv. Chim. Acta* **1993**, *76*, 2445.
(39) Magnuson, R. H.; Taube, H. *J. Am. Chem. Soc.* **1975**, *97*, 5129.

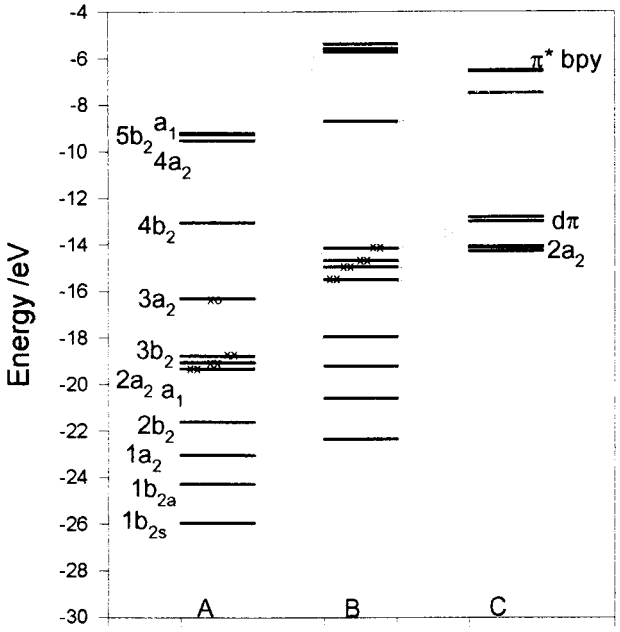

Figure 3. ZINDO/S orbital energies for (A) $[Ru(NH_3)_4(bqdi)]^{3+}$, (B) $[Ru(NH_3)_4(bqdi)]^{2+}$, and (C) $[Ru(bpy)_2(bqdi)]^{2+}$. Some lower lying σ orbitals are omitted for clarity, as are lower lying mixed bpy and bqdi levels in $[Ru(bpy)_2(bqdi)]^{2+}$.

is more complex than it appears, given that the redox processes depend upon the stabilities of both redox levels concerned. We will return to this analysis in the future.

(c) Ruthenium(III) Species. The Ru^{III} species (R = Cl, H) were also geometry optimized using ZINDO/1 and unrestricted Hartree−Fock theory (UHF), with no prior constraints on bond distances. The Ru−N(NH_3) distances of the optimized structures are about 208 pm, which is at the lower extreme of the expected range[12a,41,42] for Ru^{III}−NH_3 bond distances. The Ru−N(bqdi) distances (200 pm) are similar to those for Ru^{II}−N(bqdi).[13] The C=C bond distances within the bqdi ring (see the Supporting Information) do not alternate so clearly as they do in the quinonoid ring bound to Ru^{II}. The LUMO ($4b_2$) shows substantially greater π^* bqdi character, i.e. less d admixture for Ru^{III} relative to Ru^{II}. Clearly one expects and observes less π back-donation in the Ru^{III} species (Table 5). The percentage ruthenium is also generally lower in the SOMO ($3a_2$) than in the HOMO of the Ru^{II} species for all R, but the effect is not very pronounced. Since this is a direct reflection of Ru d−π mixing, the implication is that such mixing, while increasing for Ru^{III}, is not substantially different from the mixing in Ru^{II}, an unusual observation since π donation from bqdi to Ru^{III} might be expected to be more important than for Ru^{II}. However a closer examination does reveal enhanced d−π mixing in the Ru^{III} species. Thus the Ru contributions to the $1a_1$, $2a_2$, and $3a_2$ π orbitals are roughly the same for both Ru^{II} and Ru^{III}; however, the Ru admixture in the $2b_2$ level, which is a π−d interaction, is greater for the Ru^{III} species, for all R, than for the Ru^{II} species; it is especially large (33%) for R = OMe (Table 5). Changes in admixture to the $3b_2$ level are less clear, being greater for Ru^{III} with R = H but less with R = Cl, OMe. This may reflect the mixing with the $4b_2$ level, which has π^* character. Thus the enhanced Ru d−π mixing is revealed only in one of the two symmetry representations. The mixings in the σ levels are rather similar for both Ru^{II} and Ru^{III} for all R.

The total Ru contributions to the $3b_2$, $3a_2$, and $4b_2$ orbitals are 132, 127, and 117% for R = H, Cl, and OMe; subtraction of these values from 200% reveals, as anticipated, a greater degree of π mixing in the Ru^{III} species relative to the Ru^{II} species, again with R = OMe the most heavily mixed.

Another way to perceive the extensive mixing in this class of compounds is to note that one can no longer clearly recognize three metal-centered d(t_{2g}) type orbitals in any of the compounds. Thus, in the Ru^{II} species, for R = H, orbitals 36−40 all have substantial ruthenium, i.e. >10%, character (Tables 5 and S1), and in the Ru^{III} species, for R = H, orbitals 35−40 each have more than 10% Ru character. Because of this mixing, the splitting of the d(t_{2g}) orbitals is not so easy to define. However we can recognize that the splitting between the HOMO and HOMO-2 orbitals is really quite small for all three Ru^{II} species but quite large for the Ru^{III} species (see Figure 3 and Tables S1−S6).

Electronic Spectra−Comparison with ZINDO Predictions. (a) Ruthenium(II) Species. Table 3 shows a comparison between the observed and predicted spectra. In particular, the theory predicts, for the Ru^{II} species, only two strong bands below 43 000 cm^{-1}, and these clearly appear in the experimental data (Figures 1, S2, and 3). Thus, the overall features are reproduced though the predicted intensities are greater than actually observed experimentally; this has been noted previously with ZINDO/S calculations.[11]

Referring initially to R = H, the principal strong visible-region absorption band, ν_2, is the transition between the two levels formed by the interaction of the d_{yz} and ligand π^* orbital (π-back-donation) interaction ($3b_2 \rightarrow 4b_2$). This can be described as an MLCT transition, but there is clearly a significant $\pi \rightarrow \pi^*$ component. Previous resonance Raman data for the analogous $[Ru(bpy)_2(bqdi)]^{2+}$ species[3,15] are consistent with relatively little charge transfer in this transition, hence indicating extensive πL−d or π^*L−d mixing in the orbital concerned, as does the lack of solvatochromism in this visible-region band.[21]

The intense near-UV transition is then $3a_2 \rightarrow 4a_2$ (#39, HOMO → #41, LUMO+1) which may also be described as a mixed MLCT and $\pi \rightarrow \pi^*$ transition. In fact, this transition has more MLCT character than the visible-region absorption band.

The higher energy UV transition was not investigated in depth but appears to be assignable as #35 → #40 ($2b_2 \rightarrow 4b_2$); this can be described as $\pi \rightarrow \pi^*$ with some LMCT ($\pi \rightarrow$ d) character since the $4b_2$ orbital has a larger metal content than the $2b_2$ orbital.

The HOMO → LUMO transition itself, ν_1, #39 → #40, $3a_2 \rightarrow 4b_2$, appears as a very weak near-infrared absorption (Figure 1, insert) and also occurs between a pair of heavily mixed orbitals. Indeed, despite its weakness, it does have some $\pi \rightarrow \pi^*$ character. There is one more possible MLCT transition of the type d(t_{2g}) → π^*; this is d(a_1) → $4b_2$. It is overlap forbidden, is very weak, and was not identified in the spectra.

The other two species, R = Cl and OMe, have exactly parallel assignments though obviously with different orbital index numbers (see Tables 4 and 5). This ZINDO/S analysis fully confirms the previously proposed assignments for related species[1] but adds greater detail and insight into the nature of these transitions.

(b) Ruthenium(III) Species. Subsequently a ZINDO/S single-point calculation was carried out on all three species, using restricted Hartree−Fock theory and 800 CI states (singly

(40) Bursten, B. E.; Green, M. R. *Prog. Inorg. Chem.* **1988**, *36*, 393.
(41) Engelhardt, L. M.; Reynolds, P. A.; Sobolev, A. N. *Aust. J. Chem.* **1994**, *47*, 663.
(42) Krogh-Jespersen, K.; Zhang, X.; Westbrook, J. D.; Fikar, R.; Nayak, K.; Kwik, W.-L.; Potenza, J. A.; Schugar, H. J. *J. Am. Chem. Soc.* **1989**, *111*, 4082.

excited one-electron excitations, SECI) to predict the electronic spectra of these species.

Upon oxidation of the Ru^{II} species, for all R, the main absorption band in the visible region, ν_2, shifts to higher energy (Figures 2 and S1, Table 3). Normally one would assign such a new transition as an LMCT band. However, the ZINDO analysis paints a rather different and more complex picture. This strong band is, in fact, still MLCT, while LMCT character is associated with the next higher but rather weaker feature near 30 000 cm^{-1} (for R = H, Cl). The analog of the near-infrared band of the Ru^{II} species will also occur for these Ru^{III} species, i.e. the SOMO → LUMO transition. Its calculated energy is shown in Table 4, but except possibly in the case of R = H, it was not identified experimentally.

The principal UV feature near 40 000 cm^{-1} is predicted by ZINDO/S to be composed of many contributions. It is certainly $\pi \rightarrow \pi^*$, but it also possesses both MLCT and LMCT character. Unfortunately, the agreement between the experimental energies and the ZINDO/S-predicted energies is significantly poorer in these open-shell species than in the Ru^{II} species. Generally, ZINDO/S performs poorly with open-shell species[11] unless the excited states are very well described computationally. This leads to less confidence in the assignments. Future time-resolved resonance Raman studies should determine the issue.

The number of fairly strong bands predicted by ZINDO/S agrees essentially with the experimental spectra, and we have assumed, in making the assignments in Table 3, that the order of these transitions as predicted by ZINDO/S is the same as the experimental order. With this assumption, the actual assignments for the Ru^{III} species are essentially identical to those for the Ru^{II} species but shifted in energy. This is very reasonable, given the view of the these molecules described here. We are dealing with a pair of strongly coupled species, showing little change in the degree of metal−ligand coupling and differing only in the occupation of one orbital; we might therefore indeed anticipate parallel spectra and assignments except that the open-shell species may have some extra transitions terminating in the newly developed hole. This appears to be the case.

Comparison of Systems with Ammonia and Bipyridine. The $[Ru(NH_3)_4(bqdi)]^{2+}$ and $[Ru(bpy)_2(bqdi)]^{2+}$ systems differ as outlined in Table 4. According to the ligand electrochemical parameter theory,[7] the redox potential for the $Ru^{III/II}$ process in the bipyridine species should be about 0.76 V higher than that for the ammonia species. In fact, it is only 0.49 V greater. Assuming, reasonably, that the $E_L(L)$ parameters for bpy and NH_3 have their usual values, this must mean that the $E_L(L)$ values for bqdi are different in the two complexes. Generally, $E_L(L)$ is a constant for all species; however, it is reasonable that this may not be true for redox-active ligands such as the quinones. The $E_L(L)$ value for bqdi may well depend upon the extent of mixing with the metal center. The question of the possible variability of the $E_L(L)$ values for quinonoid ligands is under active consideration.[43] In this case, the substantial difference in the calculated values for E_L(bqdi) (0.41 for the NH_3 species and 0.28 V for the bpy species) is understood in terms of the extent of mixing in these species. Table 5 also contains mixing data for $[Ru(bpy)_2(bqdi)]^{2+}$ based upon an analysis discussed in depth elsewhere.[35] The ruthenium content in the HOMO, HOMO-1, and HOMO-2 orbitals in the NH_3 species is substantially less than for the bpy species, while the back-donation to the LUMO is greater for NH_3, though not substantially. The extent of mixing then appears greater in the NH_3 case. This is obviously because the $Ru(NH_3)_4$ moiety is a better electron donor than the $Ru(bpy)_2$ moiety. In effect then, bqdi becomes a better π acceptor with $Ru(NH_3)_4$ than with $Ru(bpy)_2$, and this is reflected in its higher E_L(bqdi) value and in the fact that it is some 400 mV more difficult to reduce (Table 4). We emphasize that these arguments must remain speculative until other redox-active ligands are analyzed.[43]

The half-bandwidth for the ν_2 transition in the Ru^{II} species is greater for the NH_3 species than for the bpy species. At first sight, this is puzzling if the degree of mixing is greater for the NH_3 species. We have argued that these transitions should be narrow because they involve little charge transfer character and hence there is little change in the nuclear coordinates between ground and excited states. This normally would ensure a narrow bandwidth. However the bandwidth depends upon the frequency of the vibrations being coexcited with the electronic transition. The principal vibration being excited, as noted from previous resonance Raman data for the bpy species,[2] is a band near 600 cm^{-1} associated with the Ru−N vibration in the RuNCCN metallacycle. However, for the ammonia species, we have shown using ZINDO that the $1b_2$ orbital is a strongly mixed π(bqdi)/$\sigma(NH_3)$ orbital. This has the same symmetry as the LUMO upon which ν_2 terminates. Thus this may well provide a pathway to couple high-frequency N−H vibrations into the ν_2 transition, providing an explanation for its broadness.

The difference in potential between oxidation and reduction of a complex, ΔE(redox) is generally related to the corresponding MLCT energy ($h\nu$(MLCT)) by a simple linear equation:[44]

$$h\nu(\text{MLCT}) = \Delta E(\text{redox}) + C \qquad (1)$$

where C is a collection of reorganization and free energy of solvation terms which, in the case of the ruthenium bipyridine system, usually sums to about 0.2−0.4 V (i.e., $h\nu$(MLCT) is usually some 1000−3000 cm^{-1} higher in energy than predicted simply by ΔE(redox)). It was recently demonstrated that when there is considerable mixing between metal and ligand, this quantity C can greatly exceed 0.2−0.4 eV.[45] This is a case in point where this difference exceeds 4000 cm^{-1} (∼0.5 eV) for bpy and 7000 cm^{-1} (0.87 eV) for NH_3 (Table 4). This is argued elsewhere[35,45] and is only partly due to the fact that ΔE(redox) is technically related to the HOMO−LUMO gap while, in these bqdi systems, ν_2 is the HOMO-1 → LUMO transition.

The actual HOMO → LUMO transition is ν_1, and this is seen (Table 4) to have an energy smaller than ΔE(redox); i.e., C, in eq 1, is negative. The Ru/L compositions of the orbitals concerned are very different in the two complexes. In the bpy molecule, the transition has considerable charge transfer character, from the HOMO with 71% Ru to the LUMO with 74% bqdi character. In the NH_3 species, however, the HOMO already has 41% bqdi character so that the transition, while still basically MLCT, has significant $\pi \rightarrow \pi^*$ character. To the extent that the actual transition deviates from an MLCT process, eq 1, which does not take into account configurational interaction, may be inappropriate. Clearly, for the bpy species, this transition has greater MLCT character than that for the NH_3 species, and the bpy complex has an energy much closer to that predicted by eq 1. Further speculation on the negative C is not useful at this time.

Dependence of Transition Energies on the Substituent R. It has often been assumed that when one changes a substituent on a ligand or changes a coligand, the direction of the shift in the charge transfer band associated with the change of substituent provides a means of determining whether the transition is

(43) Smeriglio, F.; Dodsworth, E. S.; Lever, A. B. P. Work in progress.

(44) Dodsworth, E. S.; Lever, A. B. P. *Chem. Phys. Lett.* **1986**, *124*, 152.

(45) Lever, A. B. P. *Can. J. Anal. Sci. Spectrosc.* **1997**, *42*, 24.

metal-to-ligand or ligand-to-metal. It is clear however that this simple analysis fails when extensive mixing occurs. The work of tom Dieck[46] provided an early example of this, though couched in terms of a shift in direction of the solvatochromism displayed by the transitions. Similar discussion arose in our earlier quinone studies.[1−4] In this case, the electron richness of the ligands follows the sequence R = OMe > H > Cl but the ν_2 band follows the sequence R = H > Cl > OMe. This experimental sequence is predicted by the ZINDO/S analysis. It is also true that the HOMO−LUMO gap is largest for R = H, according to ZINDO/S.

The HOMO-1 to HOMO splitting is relatively small and certainly does not account fully for the large energy difference between ν_1 and ν_2 for the Ru^{II} species. This large energy difference arises in part from a significant exchange energy contribution in the case of ν_2, as argued previously for ruthenium pentaammine species.[6a] Small variations in this exchange term, with variation in R, may be the dominating feature in deciding the sequence of ν_2. We have concluded that mixing is greater in the R = H species, and this should then possess the highest exchange energy contribution and hence the highest energy ν_2 transition, as is indeed the case. However it also possess the largest HOMO−LUMO energy gap, which would also contribute to the ν_2 transition being large for R = H. The exchange contribution to the ν_1 transition is very much smaller because the two molecular orbitals do not share a common metal-based orbital.[11]

Conclusions

Six new complexes of 4,5-disubstituted bqdi ligands with tetraammineruthenium(II) and -(III) have been synthesized and characterized. The electronic structures of these complexes have been investigated. The spectroscopic data and ZINDO analysis reveal that there is very significant π back-donation between the Ru^{II} $d(b_2)$ orbital and the π^* orbital of the ligand in the $4b_2$ LUMO. Mixing between the metal $d(a_2)$ orbital and the ligand a_2 π manifold is also extensive. In the Ru^{III} species, π back-donation is still quite strong but not quite so extensive as for Ru^{II}. Metal ($d\pi$)−ligand (π) mixing occurs extensively and especially in the $2b_2$ π orbital of the ligand. Mixing between the $\sigma(NH_3)$ orbital of b_2 symmetry and the ligand π^* b_2 orbital appears important in the $1b_2$ orbital and may be responsible for the unusual broadness of the main visible-region transition, ν_2. The ZINDO analysis paints a detailed picture of the very extensive mixing occurring in many of the MOs among metal, bqdi, and ammonia atomic orbitals. ZINDO/S is able to predict the observed electronic spectra of the closed-shell Ru^{II} species with impressive accuracy. The overall features of the spectra of the open-shell Ru^{III} species are also predicted but with less accuracy at the SECI level employed.

Acknowledgment. We thank Dr. Elaine S. Dodsworth, Dr. Scott S. Fielder, Dr. Hitoshi Masui, and Dr. Yu-Hong Tse for valuable discussions and Dr. Hitoshi Masui for experimental assistance. We also thank the NSERC for funding and Johnson-Matthey for the loan of $RuCl_3$.

Supporting Information Available: Figures showing a cyclic voltammogram of $[Ru(NH_3)_4(bqdi)]^{2+}$ (Figure S1), spectroelectrochemical oxidation (Figure S2) and reduction (Figure S3) of $[Ru(NH_3)_4(R_2\text{-}bqdi)]^{2+}$ species, electron paramagnetic resonance spectra of the $[Ru(NH_3)_4(R_2\text{-}bqdi)]^{3+}$ (Figure S4), and a plot of HOMO versus LUMO energies based upon ZINDO/S calculations (Figure S5) and Tables S1−S6, listing eigenvalues, fractional orbital mixing, and group theoretical assignments of frontier orbitals for the six complexes under discussion, as derived from ZINDO/S calculations (13 pages). Ordering information is given on any current masthead page. Pictures of some of the highly mixed MOs are presented in full color on our Web page at url www.science.yorku.ca/chem/profs/blever/blever.htm.

IC970236C

(46) tom Dieck, H.; Renk, I. W. *Angew. Chem., Int. Ed. Engl.* **1970**, *9*, 793. tom Dieck, H.; Renk, I. W. *Chem. Ber.* **1971**, *104*, 110. tom Dieck, H.; Renk, I. W. *Chem. Ber.* **1972**, *105*, 1403.